Mitigating the hosing instability in relativistic laser-plasma interactions

2016 New J. Phys. 18 053023

(http://iopscience.iop.org/1367-2630/18/5/053023)

New Journal of Physics
The open access journal at the forefront of physics

Deutsche Physikalische Gesellschaft DPG
IOP Institute of Physics

Published in partnership with: Deutsche Physikalische Gesellschaft and the Institute of Physics

OPEN ACCESS

RECEIVED
21 July 2015

REVISED
22 January 2016

ACCEPTED FOR PUBLICATION
5 April 2016

PUBLISHED
12 May 2016

PAPER

Mitigating the hosing instability in relativistic laser-plasma interactions

L Ceurvorst[1,5], N Ratan[1], M C Levy[1], M F Kasim[1], J Sadler[1], R H H Scott[2], R M G M Trines[2], T W Huang[2], M Skramic[3], M Vranic[4], L O Silva[4] and P A Norreys[1,2]

[1] Clarendon Laboratory, Department of Physics, University of Oxford, Parks Road, Oxford, OX1 3PU, UK
[2] STFC Rutherford Appleton Laboratory, Chilton, Didcot, OX11 0QX, UK
[3] Trinity College, University Cambridge, Cambridge, CB2 1TQ, UK
[4] GoLP/Instituto de Plasmas e Fusão Nuclear, Instituto Superior Técnico, 1049-0001 Lisboa, Portugal
[5] Author to whom any correspondence should be addressed.

E-mail: luke.ceurvorst@physics.ox.ac.uk

Keywords: hosing instability, hole-boring, laser-plasma interactions, plasma channeling, high energy density physics, inertial confinement fusion

Abstract

A new physical model of the hosing instability that includes relativistic laser pulses and moderate densities is presented and derives the density dependence of the hosing equation. This is tested against two-dimensional particle-in-cell simulations. These simulations further examine the feasibility of using multiple pulses to mitigate the hosing instability in a Nd:glass-type parameter space. An examination of the effects of planar versus cylindrical exponential density gradients on the hosing instability is also presented. The results show that strongly relativistic pulses and more planar geometries are capable of mitigating the hosing instability which is in line with the predictions of the physical model.

1. Introduction

The study of laser hole-boring in a relativistically underdense plasma is a subject of high interest in an extraordinarily diverse range of topics in today's laser and plasma physics research [1–4]. It has applications to ion beam generation via radiation pressure acceleration [5–9], x-ray and gamma-ray emission through betatron oscillations [10, 11], the control of the electron bunch energy in plasma wakefield accelerators [12–15], and fast ignition inertial confinement fusion [16]. The latter case was initially proposed as an alternative method to the central hot spot approach in order to achieve ignition in inertial confinement fusion. While central hot spot has recently produced results entering the alpha heating regime [17], it is still limited by hydrodynamic instabilities which prevent entry into the burning plasma regime [18–20], thus warranting the search for alternative approaches to ignition.

By contrast, fast ignition presents the opportunity to achieve high gain fusion while relaxing driver and symmetry requirements as well as avoiding several hydrodynamic instabilities present the central hot spot approach [21, 22]. It promises these enhancements by separating the compression phase from the ignition phase, rather than relying on a single driving phase as is done in conventional inertial confinement fusion. To accomplish this, a DT capsule is first compressed to ~400 g cm^{-3} with an areal density of ~2 g cm^{-2}. Ignition is then triggered by an additional short-duration (~10–20 ps) petawatt laser pulse isochorically heating the compressed target to ~10 keV [23, 24]. Upon hitting the critical surface of the coronal plasma formed during the compression phase, this high-power laser pulse then produces fast electrons of energies ~1–3 MeV that travel through the remaining plasma and deposit their energy in the dense core [25]. In the relevant intensity regime, this coupling of the laser pulse to the electrons has been experimentally shown to be relatively efficient >50% [25, 26]. However, high divergence of fast electrons produced in the coronal plasma ultimately makes the coupling of the pulse energy to the fuel a low-efficiency process by lowering the electron beam's energy flux as its

cross-section increases [27–29]. In response to this divergence, the original fast ignition scheme proposed the use of hole-boring in order to mitigate this inefficiency.

In this application of hole-boring [30–33], a high-power laser pulse is propagated into the coronal plasma between the compression and ignition pulses to create a low-density channel as far into the critical region as possible, thus minimizing the distance the ignition-stage fast electrons have to travel, and in so doing, minimizing the cross-sectional area of the beam upon reaching the compressed target and maximizing the delivered energy flux [34–36]. One of the major difficulties present in hole-boring is the hosing instability which introduces perturbations to the pulse's propagation, ultimately leading to strong tilting in the channel's direction [37–40]. This in turn causes the ignition pulse to follow the channel's path and leads to a mistargeted electron beam, thereby greatly limiting the usefulness of this scheme. It is therefore crucial to understand and minimize the effects of this instability in order for hole-boring to be an effective method of generating directed fast electron beams.

Previous studies have shown that dividing a channeling pulse into multiple ultra-short subpulses has the potential to greatly improve channel quality [41, 42]. However, these studies focused on pulses with durations less than 100 fs which are not easily obtainable on the majority of modern high-energy facilities, most of which rely on neodymium laser technology.

The primary goals of this paper are to update the physical model for the hosing instability by allowing for relativistic pulse intensities and non-negligible densities and to test this model through simulations using the relativistic particle-in-cell code, OSIRIS. Due to computational limits, research on this subject has previously been restricted to specialized, low density plasma and simulation parameters [37]. However, with recent improvements to computational resources, new facilities such as the ARCHER UK National Supercomputer [43] now allow a more comprehensive and realistic approach to be taken. In order to take advantage of these new facilities, 27 simulations were run utilizing nearly 700 000 computer core hours to study the effects of the hosing instability on relativistic laser plasma channeling at densities approaching the relativistically adjusted critical density. Since neodymium laser technology is used at the majority of high-energy, high-power laser facilities, all simulations run in this campaign feature parameters similar to those obtainable with this technology, including pulses of at least 500 fs duration and relativistic intensities up to approximately 10^{21} W cm^{-2} μm^2. These simulations will determine the viability of the multiple pulse method in this parameter regime. Additionally, these simulations will then be used to determine the effects of the density profile's geometry on the hosing instability by comparing the channels formed in radial and planar geometries.

The remainder of this paper is presented as follows. First, the physical model is presented, going through background theory on the hole-boring process in section 2 and deriving equations describing the hosing instability in section 3. Next, section 4 gives the simulation methodology, describing the 2D simulation parameters utilized throughout the paper. In section 5 the results of these simulations are then shown to illustrate the density dependence of the hosing instability and verify that these results are in line with the analytical predictions of section 3. Section 6 then applies these results to an investigation of the effects of a train of short pulses versus a single long channeling pulse. It does so by first looking at the principles behind the scheme (6.1), observing the effects of density scale length which will illustrate the importance of the hosing instability's density dependence (6.2), and notes an observed self-correction mechanism (6.3) as well as the effects of the initial plasma profile, in particular the curvature of the initial plasma densities (6.4). The validity of these simulations is shown in the appendix. Finally, the paper is concluded with a brief discussion and summary of these results.

2. Hole-boring

When a laser pulse is incident upon a plasma, it will expel electrons from its path through the ponderomotive force given by

$$\vec{f}_{\rm P} = -(e^2/4m\omega^2)\nabla|\vec{E}|^2, \tag{1}$$

where e is the electron charge, m is the electron mass, ω is the pulse angular frequency, and $\vec{E}$ is the electric field of the pulse. Further, according to the stationary model [44, 45], the pulse will completely evacuate the electrons from the plasma channel when the laser pulse power is above the channeling power, $P_{\rm ch} = [17.7 n_{\rm c}/n]\,GW$ where $n_{\rm c}$ is the non-relativistic critical density and n the electron density [46]. This derivation will limit its analysis to pulses with power above $P_{\rm ch}$ incident upon near- or over-dense plasma regions, where the pulse will no longer be able to propagate forward significantly. In this regime, the radiation pressure acts as a piston that accelerates the plasma forward, thereby creating a low-density channel while the ions and electrons accelerated out of the region travel at approximately the same velocity, passing through the unperturbed plasma and leaving it practically neutral [5].

In the channel front's frame, through number conservation and by relating the laser pressure to the momentum flux, the hole-boring velocity in an over-dense plasma may be derived as

$$v_{\rm hb}^{+}/c = a_0\sqrt{n_{\rm c}Zm/2nM}\,, \tag{2}$$

where Z the charge state, M the ion mass, and $a_0 = e|\vec{E}|/mc\omega$ is the dimensionless vector potential [47–49]. Now defining the dimensionless piston parameter $\Xi = I/\rho c^3$, where ρ is the mass density, this may be simplified to $v_{\rm hb}^{+}/c = \sqrt{\Xi}$ [50].

In order to find the over-dense hole-boring depth, $d_{\rm hb}^{+}$, of a pulse of fixed intensity and duration in the limit where n is and comparable to $n_{\rm c}$, all that remains is to integrate the hole-boring velocity over the duration of the pulse's propagation. In the simplest case of constant density, all that is required is to multiply the over-dense hole-boring velocity by the duration of the pulse, τ, to obtain

$$d_{\rm hb}^{+} = c\tau\sqrt{\Xi} = a_0 c\tau\left(\frac{n_{\rm c}}{2n}\frac{Zm}{M}\right)^{1/2}. \tag{3}$$

It is worth observing that the derivation of equation (3) assumes that the hole-boring velocity is non-relativistic (i.e. $I \ll \rho c^3$). To allow for relativistic hole-boring speeds, the number density and mass in the plasma momentum flux must each be multiplied by a Lorentz factor and the intensity of the pulse will undergo a Doppler shift between the laboratory and channel front frames. These combined effects result in a lowered hole-boring velocity of $v_{hb,\gamma}^{+}/c = \sqrt{\Xi}/(1+\sqrt{\Xi})$. Additionally, due to the fact that the rear of the pulse will now require extra time to reach the channel front, the pulse's propagation time in the laboratory frame will be larger than the pulse duration according to $\tau_\gamma = \tau/(1 - v_{hb,\gamma}^{+}/c) = (1+\sqrt{\Xi})\tau$ [50]. Note however that by multiplying the relativistically correct hole-boring velocity by the propagation time yields the exact same equation as equation (3), thereby showing that this equation is consistent at all relevant intensity levels.

While these equations are fairly robust at higher densities, discrepancies arise at densities below critical where the assumptions made in deriving equation (3) break down [51–53]. A more accurate description of the under-dense hole-boring depth, $d_{\rm hb}^{-}$, may be obtained by noting that the laser pulse initially interacts with the electron species primarily through the ponderomotive force, and after initially transferring its energy to electron quiver motion, this energy is then subsequently transferred to several other forms which constitute the complex absorption process [54, 55]. As a result, one may approximate $d_{\rm hb}^{-}$ by equating the deposited pulse energy to the quiver energy given to the electron species. To find this value, note that the energy given to each electron through the ponderomotive force is found by integrating equation (1), $\int\vec{f}_{\rm P}\cdot{\rm d}\vec{r} = (1/4)a_0^2mc^2$. Multiplying this by the number of electrons in the channel gives $U_{\rm P} = (1/4)a_0^2mc^2d_{\rm hb}^{-}\bar{n}A$, where A is the cross-sectional area of the pulse, the volume of the channel has been approximated as $V = Ad_{\rm hb}^{-}$, and the average density $\bar{n} = V^{-1}\int n\,{\rm d}V$

This value needs to be equated to the amount of laser energy used to create the channel, $U_{\rm L} = \zeta IA\tau = (1/2)\zeta n_{\rm c}mc^3a_0^2A\tau$, where ζ is the coupling parameter indicating the fraction of the pulse energy contained within the channel. This value can vary in 2D simulations from $\zeta \approx 1$ in p-polarization [54] to values as low as $\zeta \approx 0.6$ in s-polarization [56]. The difference between the two polarizations lies in the escaping pulse energy in s-polarization case which may then continue on to form soliton-like structures [56–60]. Equating $U_{\rm L} = U_{\rm P}$, gives the under-dense hole-boring depth as

$$d_{\rm hb}^{-} = 2\zeta c\frac{n_{\rm c}}{\bar{n}}\tau \tag{4}$$

Despite the simplistic assumptions made in deriving this equation, it has been shown to be a reasonable estimate for sub-picosecond pulses in relativistically transparent plasmas [54]. However, it should be noted that for higher densities and longer pulse durations, the channel walls will become over-critical, thereby reducing the hole-boring velocity and depth to the corresponding overdense values.

3. The hosing instability

In addition to understanding how deep a pulse travels into a plasma to form a channel, it is also important to understand how the hosing instability will in turn cause a channel to change its direction. As a laser pulse propagates through a plasma, its path will undergo slight perturbations due to transverse asymmetries in the phase velocity about the pulse's centroid. These asymmetries then lead to a tilting of the pulse's wavefront and thus its propagation direction. Therefore, in order to derive these asymmetries, it is important to first derive an equation for the phase velocity when the relevant parameters are perturbed.

The derivation presented here is based on the physical picture given in [61] but with the addition of the allowance of larger densities and ultra-intense ($a_0 \gg 1$) pulses. Highly relativistic pulses are beneficial as they allow a magnetic field to be seeded in front of the channel which can subsequently be used to collimate fast electron beams generated by trailing pulses [62]. Additionally, they reduce the impact of external density

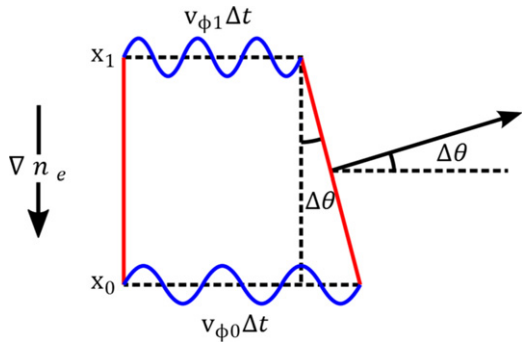

Figure 1. Schematic of phase velocity asymmetries affecting the propagation of a pulse in an underdense plasma.

perturbations on the phase velocity and therefore the hosing instability. This can be seen by noting that the index of refraction is given as $\eta = (1 - \omega_p^2/\gamma\omega^2)^{1/2} = (1 - n/n_{\gamma c})^{1/2}$, where ω_p is the electron plasma frequency, $\gamma = (1 + a_0^2)^{1/2}$ is the Lorentz factor for a circularly polarized beam, and $n_{\gamma c} = \gamma n_c$ is the relativistically adjusted critical density.

To begin, assume an ideal case where a pulse with a table-top transverse profile is propagating through an underdense plasma. Then assuming the density, frequency, and intensity initially vary little in the region of interest, one may set $n = n_0 + n_1$, $\omega = \omega_0 + \omega_1$, and $a_0^2 = a_{00}^2 + a_{01}^2$ where subscripts 0 denote the fixed components and subscripts 1 denote the varying components. Because the maximum frequency shift of the pulse as it passes through the plasma is given as $\omega_1/\omega_0 \propto (\omega_p^2/\omega^2)n_1/n_0$ [63] and phenomena such as the filamentation instability only become appreciable with density modulations of the order $n_1/n_0 \sim 1 - e^{-\gamma_p} \to 1$ for high intensities, where γ_p is the ratio of the ponderomotive pressure to the thermal pressure [64], confining the analysis to times such that $n_1 \ll n_0$ will result in $\omega_1 \ll \omega_0$ and $a_{00}^2 \ll a_{01}^2$. Then using these values, substituting into the phase velocity equation, $v_\phi = c\eta^{-1}$, and linearizing shows

$$\begin{aligned}\frac{v_\phi}{c} &= \left[1 - \frac{n_0}{n_{\gamma c0}}\left(1 + \frac{n_1}{n_0} - \frac{1}{2}\frac{a_{01}^2}{\gamma_0^2} - 2\frac{\omega_1}{\omega_0}\right)\right]^{-1/2} \\ &= \left[\frac{n_{\gamma c0} - n_0}{n_{\gamma c0}} - \frac{n_0}{n_{\gamma c0}}\left(\frac{n_1}{n_0} - \frac{1}{2}\frac{a_{01}^2}{\gamma_0^2} - 2\frac{\omega_1}{\omega_0}\right)\right]^{-1/2} \\ &= \sqrt{\frac{n_{\gamma c0}}{n_{\gamma c0} - n_0}}\left[1 + \frac{1}{2}\frac{n_0}{n_{\gamma c0} - n_0}\left(\frac{n_1}{n_0} - \frac{1}{2}\frac{a_{01}^2}{\gamma_0^2} - 2\frac{\omega_1}{\omega_0}\right)\right],\end{aligned} \tag{5}$$

where $\gamma_0 = (1 + a_{00}^2)^{1/2}$, $n_{c0} = m\epsilon_0\omega^2/e^2$, and $n_{\gamma c0} = \gamma_0 n_{c0}$. In the last step, it has been assumed that n_0 is sufficiently underdense so that $(n_{\gamma c0} - n_0)/n_0 \gg (n_1/n_0) - (a_{01}^2/2\gamma_0^2) - (2\omega_1/\omega_0)$ which is a reasonable restriction as it was assumed that $n_1 \ll n_0$ and similar for the other values.

In order to see how a phase velocity asymmetry affects the propagation direction of a pulse, consider a pulse with a table-top transverse profile propagating through a plasma with a slight perturbation to the electron density such that there is a transverse density gradient as illustrated in figure 1. Let θ be the angle between the pulse's current trajectory compared to its original trajectory and let $\hat{x}$ be the transverse direction. As can be seen from this figure, the change in propagation direction is given by $\tan(\Delta\theta) = (v_{\phi 0} - v_{\phi 1})\Delta t/(x_0 - x_1)$, or by letting Δt tend towards zero

$$\frac{\partial\theta}{\partial t} = -\frac{\partial v_\phi}{\partial x}. \tag{6}$$

In general, the pulse frequency and intensity will be symmetric about the centroid of the pulse, and so they will have little effect on the hosing instability [61]. Therefore, when inserting equation (5) into equation (6), only the density term will remain.

$$\frac{\partial\theta}{\partial t} = -\frac{c}{2}\sqrt{\frac{n_{\gamma c0}n_0^2}{(n_{\gamma c0} - n_0)^3}}\,\frac{\partial}{\partial x}\frac{n_1}{n_0}. \tag{7}$$

Assuming that θ is small, the rate of change of the displacement of the centroid is given as $\partial_t X_c = v_\phi\theta$, where X_c is the transverse location of the centroid and where the short-hand $\partial_\alpha = \partial/\partial\alpha$ has been used for legibility. Taking the derivative with respect to time of this equation and noting that $\theta\partial_t v_\phi \ll v_\phi\partial_t\theta$ since n and therefore v_ϕ vary little in the region of interest and $\theta \ll 1$, it can be shown that

$$\frac{\partial^2 X_c}{\partial t^2} = -\frac{1}{2}c^2\frac{n_0}{n_{\gamma c0}}\left(1 - \frac{n_0}{n_{\gamma c0}}\right)^{-2}\frac{\partial}{\partial x}\frac{n_1}{n_0}. \tag{8}$$

Note that in the limit $a_0 \ll 1$ and $n \ll n_c$, equation (5) becomes $v_\phi/c = 1 + (n_0/2n_{c0})(1 + n_1/n_0 - \langle a_0^2\rangle/2 - 2\omega_1/\omega)$ by Taylor expanding the square root term, and equation (8) becomes $\partial_t^2 X_c = -(1/2)\,(c^2 n_0/n_{c0})\,\partial_x(n_1/n_0)$ which both exactly match the equations found in [61, 65].

At this point, the density response equation must be chosen to accurately reflect the effects of the interacting laser pulse on the plasma's density profiles. For short-pulses, the first-order response of the density profile due to the pulse is given by [65]

$$\left[\frac{\partial^2}{\partial\psi^2} + \omega_p^2\right]\frac{n_1}{n_0} = \frac{\partial^2}{\partial\psi^2}\frac{\langle a_0^2\rangle}{2}, \tag{9}$$

where $\psi = t - z/c$ is the speed-of-light frame longitudinal axis. This equation assumes that the ion motion due to direct acceleration by the laser pulse is negligible compared to the electrostatic force from the charge separation of the electron and ion species [66], thereby limiting the scope of the rest of this section to pulses whose intensity is not sufficient to accelerate ions up to the relativistic regime ($I < 10^{24}$ W cm^{-2}).

Then in the long wavelength regime ($\partial^2/\partial\psi^2 \ll \omega_p^2$), when assuming a super-Gaussian intensity profile for the pulse, the density gradient caused by the pulse itself is given as

$$\frac{\partial}{\partial x}\frac{n_1}{n_0} = \frac{\langle a_0^2\rangle}{2W^2(\omega_p^2/\gamma)}\frac{\partial^2 X_c}{\partial\psi^2}, \tag{10}$$

where W is the spot size of the pulse. Inserting this into equation (8)

$$\frac{\partial^2 X_c}{\partial t^2} = -\frac{c^2}{4W^2\omega_0^2}\frac{1}{(1 - n_0/n_{\gamma c0})^2}\langle a_0^2\rangle\frac{\partial^2 X_c}{\partial\psi^2}. \tag{11}$$

This equation matches the hosing equation presented in the literature [61, 67] but with the addition of a factor of $(1 - n_0/n_{\gamma c0})^{-2}$. This is an important distinction as many applications of hole-boring require channeling through moderate to near-critical densities. It shows that while pulses tend to hose more at higher densities, relativistic intensities are capable of mitigating this effect through the increase of the relativistic critical density. This is vital as equation (8) shows that higher intensities are required in order to overcome the external density perturbations which are present in any ablated plasma, making high intensities a viable approach to hole-boring in practical scenarios. It is worth noting that this equation reduces to exactly the previously presented hosing equations when making the matching assumption of $n \ll n_c$.

Other density response equations and intensity profiles may be chosen to produce slightly different results from equation (11), though equation (8) will still need to be utilized in order to determine the acceleration of the centroid, thereby maintaining the density dependence. In weakly relativistic hole-boring for instance, a more accurate description may be obtained by setting the ponderomotive and wakefield potentials equal to each other, giving $n_1/n_{\gamma c0} \approx (c^2/\omega_0^2)\nabla^2 a^2/4$. Combined with a half-cycle cosine function for the intensity profile, to first order in X_c, this produces a harmonic oscillator equation with [68]

$$\lambda_{hosing} \approx \frac{4\sqrt{2}\,\lambda_0^2}{a_0 W}\left(\frac{n_{\gamma c0}}{n_0}\right)^{3/2}\left(1 - \frac{n_0}{n_{\gamma c0}}\right). \tag{12}$$

This shows that at higher densities, the hosing wavelength will be shorter than previously predicted due to the increased transverse acceleration predicted in equation (8), tending towards zero at the relativistically adjusted critical density. Further adjustments may be made to the density response equations, including the effects of ion motion on the electron density which has been shown to reduce hosing levels when using non-relativistic intensity laser pulses [69], though these effects are outside the scope of this paper.

4. Methods

In order to test the validity of this physical model, an extensive set of two-dimensional simulations were run using the simulation code, OSIRIS, a two-dimensional, fully relativistic, massively parallel particle-in-cell code. All results from this program are dimensionless to allow for scaling, requiring a fundamental wavelength to be chosen in order to convert these results into physical units. While the results given here are from 2D simulations, this is expected to be sufficient as quantitative improvements have been shown to exist in 3D particle-in-cell simulations while maintaining qualitatively similar results [70].

All simulations in this paper utilize periodic boundary conditions on the top and bottom of the simulation boxes and fully particle absorbing conditions on the left and right boundaries. The pulses used in these

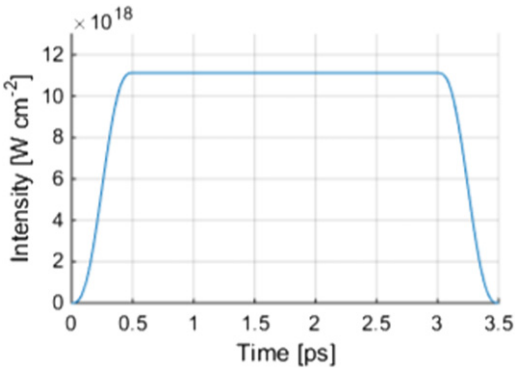

Figure 2. Temporal intensity profile for all pulses used in section 5.

simulations enter the windows from the right boundaries, have Gaussian longitudinal rise and fall envelopes, and are focused at $109.2\lambda_L$ to a spot diameter of $10\lambda_L$, where λ_L is the laser wavelength. Their transverse spatial profile is super-Gaussian in intensity.

Section 5 utilizes circularly polarized pulses which propagate into a $114.0\lambda_L \times 95.0\lambda_L$ window. The pulses have maximum intensities corresponding to $a_0 = 3$ and are propagated into plasmas of constant densities corresponding to $0.17n_{\gamma c}$, $0.20n_{\gamma c}$, $0.25n_{\gamma c}$, and $0.40n_{\gamma c}$. The spatial grid used in each each simulation was chosen to match the Debye length for a 10 keV plasma which correspond to grid sizes of 3750×3150, 4050×3400, 4550×3800, and 5750×4800 cells respectively.

In section 6 s-polarized pulses again enter from the right side of a $189.9\lambda_L \times 142.5\lambda_L$ window. The density at the focus of the pulses is $0.1n_c$. Each pulse has a peak intensity corresponding to $a_0 = 20$. The spatial grid contains $10\,000 \times 7500$ cells with 3×3 particles per cell and an initial electron temperature of 10 keV in order to give a Debye length of approximately $0.006\lambda_L$ at $15\ n_c$.

For ease of reading, the remainder of this paper will convert simulation parameters into physical units assuming the fundamental laser wavelength to be $\lambda_0 = 1.053\ \mu$m. However, the results may be generalized by multiplying both time and distance by λ_L/λ_0 and maintaining the values of densities in terms of n_c and intensities in terms of a_0.

5. Verification of density dependence

In this section, particle-in-cell simulations are used to study the density dependence of the hosing instability. All pulses used in this section have a rise and fall time of 0.5 ps and maintain their maximum intensity for 2.5 ps, giving a FWHM duration of 3.0 ps. An illustration of this temporal profile is shown in figure 2. In each simulation, a single pulse is propagated from the right of the simulation window into a $100\ \mu$m $\times$ $100\ \mu$m plasma layer of constant density. This plasma layer has a $10\ \mu$m exponential density fall-off with $2\ \mu$m scale length on either side of it in order to avoid any unphysical effects from the absorbing boundaries.

In order to verify the density dependence given in equation (8), the density of the plasma layer was varied, and simulations at $0.17n_{\gamma c}$, $0.20n_{\gamma c}$, $0.25n_{\gamma c}$, and $0.40n_{\gamma c}$ were run where $n_{\gamma c} = \gamma n_c$ is the relativistic critical density. The results of these simulations are shown in figure 3 after 4 ps of simulation time, giving the pulses enough time to complete their propagation through the plasma and the channels have neared stagnation. As can be seen, the channels in these simulations decrease in depth as the density goes up as one would expect from equation (4).

Additionally, several bubble-like structures known as solitons can be seen in these simulations. These solitons are the results of laser pulse energy escaping the channel and propagating through the plasma. As these divergent beamlets continue to propagate through the plasma, they adiabatically decrease in energy, leading to a redshift of the radiation which causes the walls around them to become over-critical and trapping the pulse energy inside to form a soliton [59, 60]. As the light couples with the electrons and ponderomotively keeps the electron density negligible within the soliton, a charge gradient is formed between the electrons and ions. The ions then are accelerated out of this bubble region leading to what is known as a post-soliton [71, 72].

In order to determine the offset of the channels, transverse line-outs were taken at the points indicated by vertical magenta lines in figure 3. Based on these lineouts, the magnitude of the displacement from the original axis of propagation of the pulse was determined and the results are plotted in figure 4 and compared to the additional density factor of $(1 - n/n_{\gamma c})^{-2}$ that was derived in equation (11).

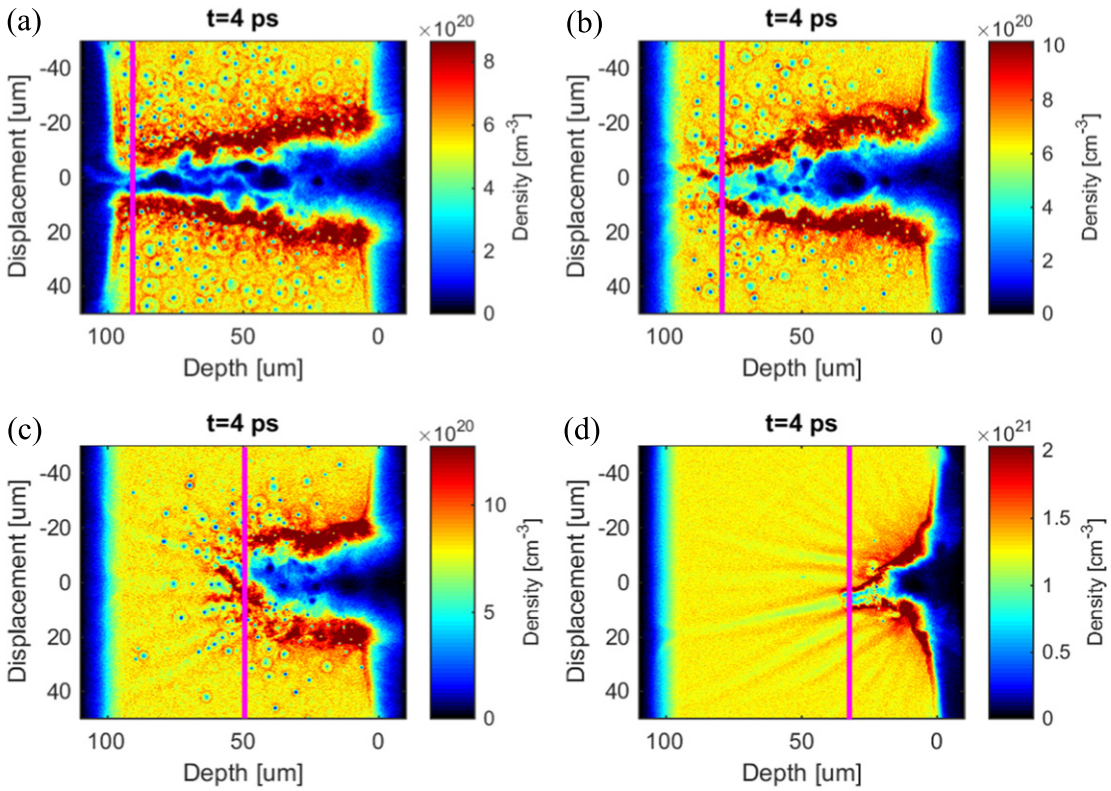

Figure 3. The electron density profiles for a 3 ps pulse propagating from the right boundary through a plasma of density (a) $0.17n_{\gamma c}$, (b) $0.20n_{\gamma c}$, (c) $0.25n_{\gamma c}$, and (d) $0.40n_{\gamma c}$. The magenta vertical lines superimposed on each image indicate the point where the displacement of the channel was measured for each simulation.

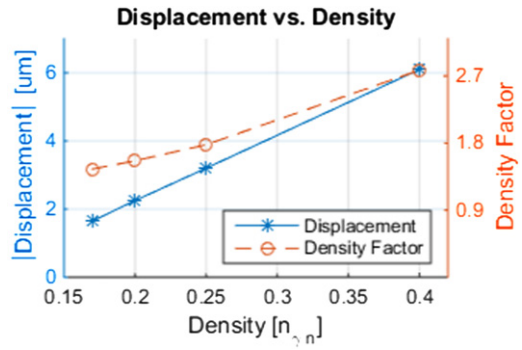

Figure 4. Final magnitude of the displacement of the channels in figure 3 as a function of density is plotted in solid blue. The orange dashed line represents the density factor $(1 - n/n_{\gamma c})^{-2}$ derived in equation (11).

As can be seen, the displacement of the channels indeed increases as a function of density as predicted by equation (11). However, this displacement increases much more rapidly than the density factor would indicate. This can be attributed to the difference between the phase velocity of the laser pulse and the slower hole-boring velocity. The transverse acceleration of the pulse is given in the speed of light frame independent from the hole-boring velocity. As the hole-boring velocity is lower in higher density plasmas, this will cause the channel to hose at an increased angle. Therefore, $\partial^2_\psi X_c$ will be greater in higher density simulations and by equation (8), the total displacement will be increased over lower density simulations beyond what the density factor may suggest.

6. Application—pulse number

In this section, two sets of simulations utilizing the simulation parameters listed in section 4 are compared, one set using a single pulse and the other set using a train of multiple shorter pulses. The goal of this analysis is to

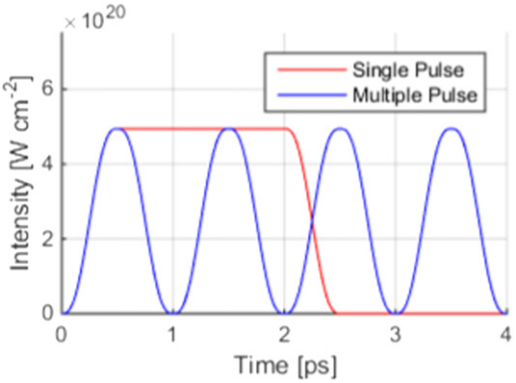

Figure 5. Temporal intensity profiles for the single pulse simulation (red) and the multiple pulse simulation (blue).

determine if the multiple pulse scheme proposed by [41, 42] is applicable to the neodymium-based laser technology found in several high-energy, high-power facilities today, and to illustrate the importance of increased hosing at higher densities shown in the previous sections.

As the physical model shows, the hosing instability increases over the duration of the pulse propagation time through the plasma. Therefore in order to be successful, the individual short pulses which constitute the multiple pulse scheme must have ceased propagation through the plasma before the hosing instability has had time to significantly alter each pulse's trajectory through the mechanisms described in the derivation of the underdense hole-boring depth, equation (4). Further, in an effort to minimize the channel filamentation, the spot size of the pulse should be kept to a minimum [73] but because of this, relativistic intensities are required in order to remain above the channeling power threshold, P_{ch}, discussed in section 2.

The simulations presented in this section all have pulses propagating from the right of the windows into a radial exponential density profile given by $n = 20n_c \exp\left[-(\sqrt{x^2 + z^2} - 100\ \mu\text{m})/L\right]$ where x is the transverse component, z the longitudinal component, and L the scale length. The simulation window is $200\ \mu\text{m} \times 150\ \mu\text{m}$ with $100\ \mu\text{m} \leqslant z \leqslant 300\ \mu\text{m}$ and $-75\ \mu\text{m} \leqslant x \leqslant 75\ \mu\text{m}$, so that the maximum initial density in the simulation window is $20n_c$ with a radial fall-off centered $100\ \mu$m to the left of the window. The single pulse simulations utilize a pulse with a rise and fall time of 0.5 ps each with a flat peak time of 1.5 ps while, unless otherwise noted, the multiple pulse simulations use four pulses, each with 0.5 ps rise and fall time and a temporal separation between peak intensities of 1.0 ps. This maintains equal energy and peak intensity between simulations. An illustration of these intensity profiles is shown in figure 5.

6.1. Proof of principle

To begin the investigation, the scale length of the density profiles was set to $L = 50\ \mu$m in order to allow the pulses to enter a sub-critical plasma. The evolution of a typical single pulse simulation is shown in figure 6. As can be seen from this figure, the pulse propagates through the plasma relatively unperturbed until approximately $z = 150\ \mu$m where significant hosing begins to occur. However, the pulse then begins to self-correct itself around 1.5 ps into the simulation at which point it is able to continue propagation in its original direction. A more detailed discussion of this behavior is presented in section 6.3.

In order to compare the differences between simulations, figure 7 shows the overlay of the channel formation of the two pulses. The data shown was calculated by thresholding the density profiles at 1.5 ps below 50% of the initial density. As can be seen in this figure, both simulations experience similar levels of hosing, showing virtually no improvement in the multiple pulse simulation over the single pulse simulation. This is due to the multiple pulse scheme's pulses not having a short enough duration. As discussed at the beginning of this section, in order for the multiple pulse method to be effective, the leading pulse should cease channeling before hosing begins. If it does not, trailing pulses will follow the initial channel and begin channeling into the remaining plasma in the direction of the hosing of the first pulse. Looking at figure 6(b), it is clear that in order to meet this criterion, the pulse should have stopped channeling before approximately $z = 175\ \mu$m. Integrating the initial density profile from $z = 175\ \mu$m to $300\ \mu$m and $x = -15\ \mu$m to $15\ \mu$m and dividing by the corresponding volume, the average density originally in the channel is approximately $1.6n_c$. Since this is a short-pulse relativistically under-dense simulation similar to the scenario in [54], this value is then substituted in as n along with $d_{hb}^{-} = 125\ \mu$m into equation (4) to find the maximum pulse duration with this initial density profile to be approximately 0.37 ps in order to avoid hosing in the initial pulse.

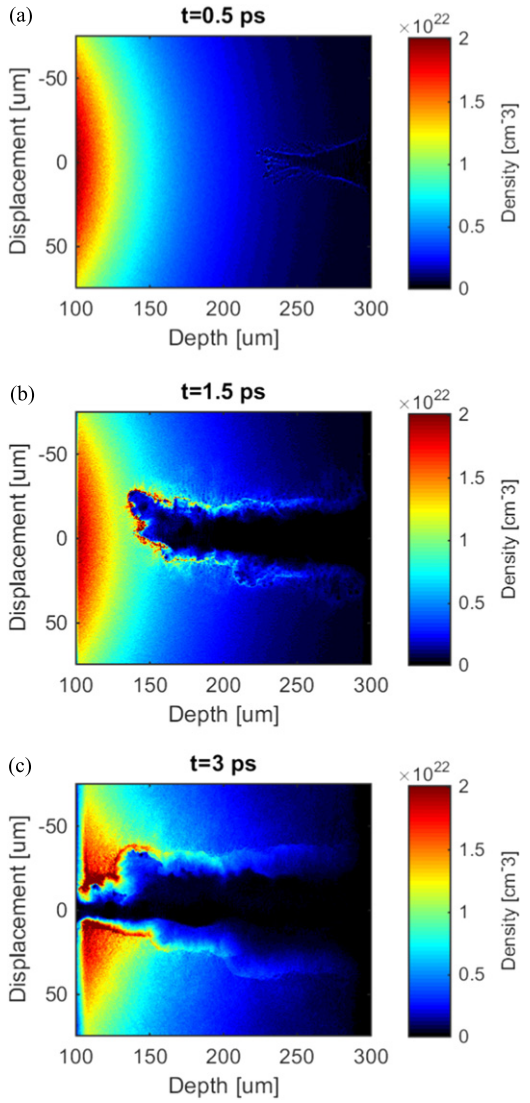

Figure 6. Electron density of the single pulse simulations at (a) 0.5 ps, (b) 1.5 ps, and (c) 3.0 ps. Case (b) shows significant hosing in the pulse's propagation. However, this has self-corrected by case (c) due to the high ponderomotive pressure of the incoming relativistic pulse.

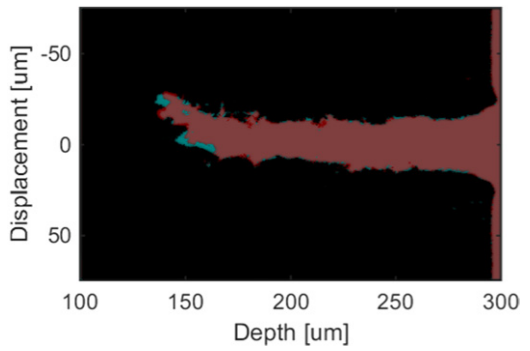

Figure 7. Overlay of the single pulse simulation (blue) and the multiple pulse simulation (red) thresholded below 50% of their initial density profiles. As can be seen, the two simulations experienced similar amounts of hosing at this point, thus showing virtually no improvement in the multiple pulse simulation over the single pulse simulation.

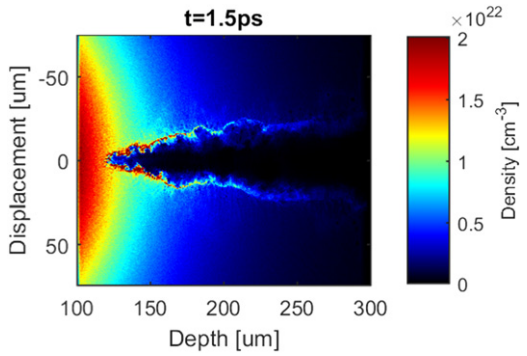

Figure 8. Electron density of the 0.25 ps pulse simulation at 1.5 ps into the simulation. The resulting channel is significantly straighter than the results presented in figures 6 and 7.

Based on these calculations, an additional simulation was run using the same density profile, but this time employing a series of eight 0.25 ps FWHM Gaussian pulses with a separation between peaks of 0.6 ps. This pulse duration is below the capabilities of neodymium-based facilities, but it is interesting to verify the validity the principle behind the multiple pulse scheme nonetheless.

While minor levels of hosing are detectable throughout each pulse's propagation, the amplitude of the hosing never has enough time to significantly effect a redirection of the overall pulse propagation. The electron density for this simulation is shown in figure 8 after 1.5 ps of propagation time in order to match the timings in figures 6 and 7. As can clearly be seen, the hosing present in the previous two simulations has been successfully eliminated through the use of multiple pulses. The channel formation continues in the original direction of propagation through the end of the window, thereby showing the validity of the multiple pulse scheme. However, in addition to the unrealistically short pulse durations, the density scale length in an inertial confinement fusion implosion are typically on the order of hundreds of microns [20], meaning that more work is required in order to verify the applicability of this scheme to inertial confinement fusion.

6.2. Scale lengths

In order to better determine the feasibility of the multiple scheme in realistic scenarios, four additional simulations were carried out using the single 2 ps pulse and four 0.5 ps pulses as discussed at the beginning of this section. Each of these pulse configurations was propagated into plasmas with scale lengths of $L = 100$ μm and 200 μm. The increased scale lengths would cause the pulses to propagate through plasmas of higher density, thereby lowering their individual hole-boring depths as predicted by equations (2) and (4). However, as shown in sections 3 and 5, the levels of hosing should increase as well, thus introducing a competing effect.

In both of these density profiles, the performance of the multiple pulse scheme declined as the scale length increased. Figure 9 shows the resulting density profiles for the single pulse and multiple pulse configurations in the 200 μm scale length density profile at various times, approximately matching the hole-boring depths. As can be seen qualitatively, the single pulse channel experiences small amounts of hosing at various times along its propagation but is able to quickly self-correct itself before any significant displacement is achieved. The multiple pulse scenario on the other hand does experience severe hosing around $z = 220$ μm.

The poor performance of the multiple pulse scheme is due to the decreasing intensity at the tail of the pulse. The relativistically induced transparency is reduced as the pulse continues to lower in intensity, thus increasing $n/n_{\gamma c}$, and thereby greatly increasing the effects of hosing as predicted by equation (8). Eventually this leads to the plasma being over-critical, thereby preventing further propagation. This accounts for the sharp bend in the channel in figure 9(d). Indeed, each case of strong hosing in these multiple pulse simulations corresponded with the completion of a short pulse. Therefore, while the multiple pulse scheme could be useful below critical density or with pulses with extremely short rise and fall times, it is not well-suited for propagation in relativistically transparent plasmas due to the increased levels of hosing present at higher relativistically adjusted densities.

6.3. Ponderomotive self-correction

Throughout the simulations in this section, after a pulse initially undergoes hosing, it is able to quickly correct itself. This is a result of the extremely high ponderomotive pressure at $a_0 = 20$ which initially seeds a forward-facing channel by nearly immediately evacuating the electrons in front of it. An example of this is visible in figure 6(b). If the channel wall in front of the pulse is overdense, as has been the case with the simulations found in this section, then this process is similar to the momentum flux transfer described in the derivation of the

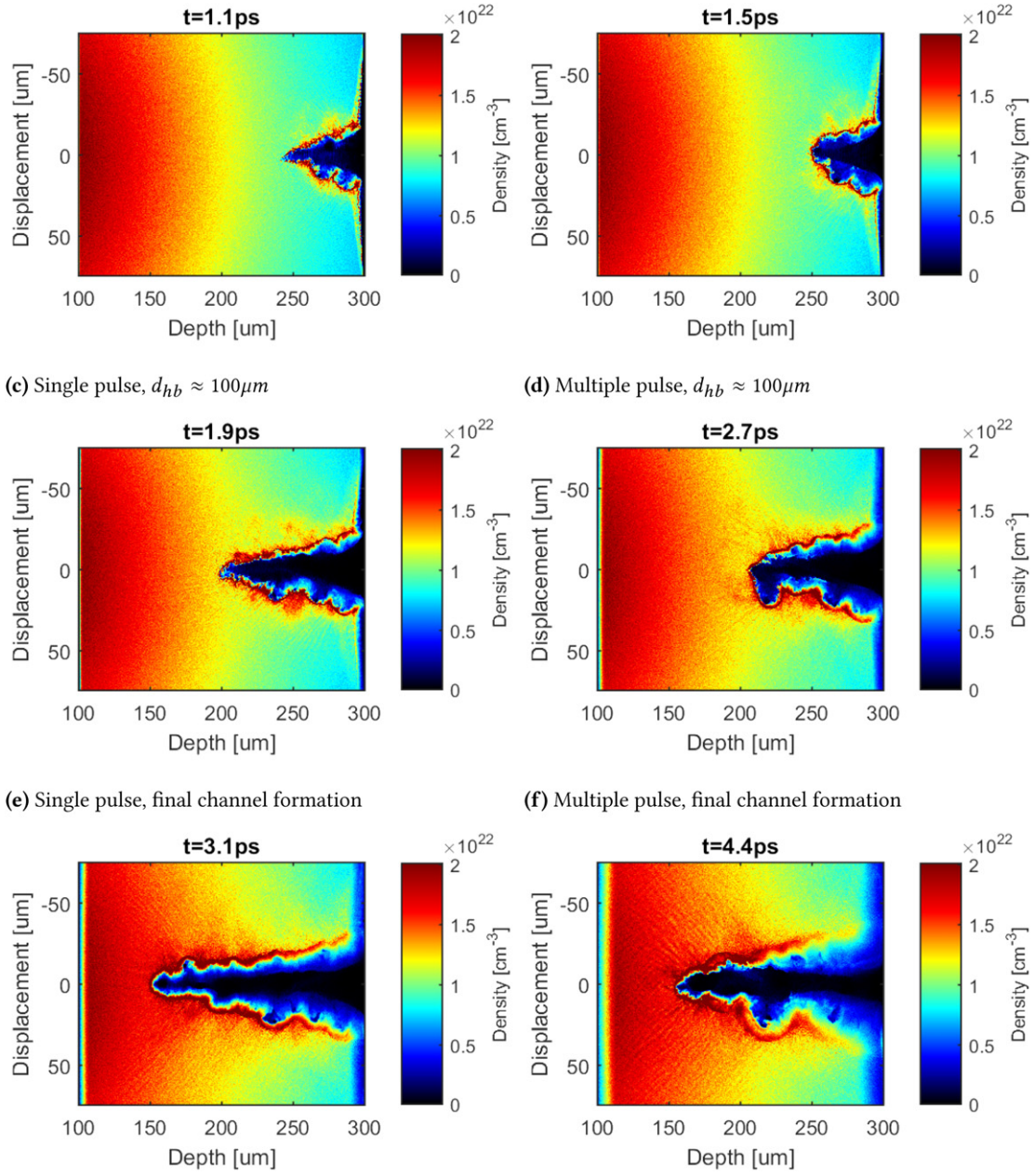

Figure 9. The electron density profiles for the single pulse (left) and multiple pulse (right) simulations using a density scale length of 200 μm. The various times and propagation distances are given in each subcaption.

overdense hole-boring velocity, equation (2). After creating the initial 'dent' in the channel wall, the rest of the pulse is able to focus further since once in this 'dent', the plasma density is then locally symmetric and the pulse is able to proceed in its original propagation direction. As a result, by the time the pulse reaches the rear of the simulation in figure 6(c), it has fully self-corrected and the displacement is no longer discernible.

This behavior will be more evident at higher intensities even if the initial density profile as a function of $\tilde{n} \equiv n/n_{\gamma c}$ is kept constant between scenarios. To see this, note from equation 2 that the overdense hole-boring velocity which drives this process can be written $v_{hb}^{+} \propto a_0/\sqrt{n} \propto \sqrt{a_0/\tilde{n}}$. Therefore, higher intensity pulses will self-correct faster than their lower intensity counterparts, and by doing so, a smaller fraction of the total pulse energy will have gone into the creation of these branching filaments.

From equation (8), it can also be seen that given an external perturbation, n_1/n_0, relativistic pulses will experience less displacement due to the effects of relativistic transparency and the resulting increase to $n_{\gamma c}$. Thus, high intensity pulses are able to give additional control of the channel, and the additional energy cost of using high intensity pulses [37] is mitigated by the speed of the self-correction.

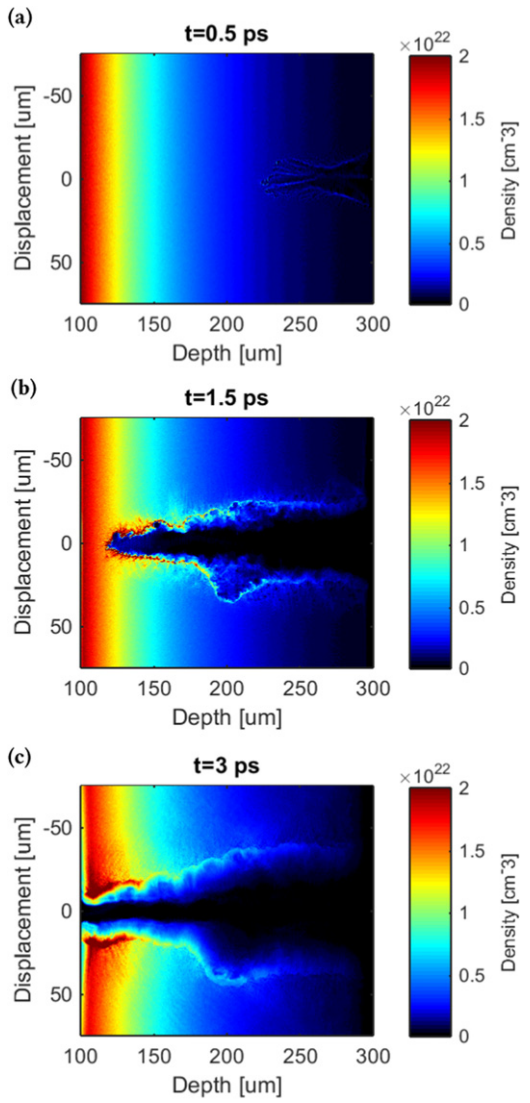

Figure 10. Electron density of the planar density profile simulation at (a) 0.5 ps, (b) 1.5 ps, and (c) 3.0 ps. As can be seen, there is virtually no hosing through the entire evolution of the simulation, thereby showing less hosing in planar versus radial density profiles.

6.4. Geometry dependence

As a final note, in addition to investigating the number of subdivided pulses and plasma scale length, it is important to analyze the effects of the initial density profile on the hosing instability. One would expect a more planar density profile around the critical density in a larger-scale experiment as much more matter is ablated causing the critical density to be reached at a much greater radius from the target center, while smaller-scale experiments would experience a much more radially dependent density profile. Therefore, an additional simulation was run in a planar exponential density profile which otherwise matches the parameters of the single pulse simulation with $L = 50\ \mu$m. The new density profile in this run is given as $n = 20n_c \exp(-z/L)$, where x is again the transverse component and z the longitudinal component. This density profile is identical to the profiles used above but without the transverse component dependence.

The temporal evolution of this simulation is shown in figure 10. After 1.5 ps, it appears as though some hosing did occur around halfway through the simulation window. However, this is the result of the initial filamentation of the beam as it came into focus and is not a change in the main pulse's trajectory. This is further exemplified as the density in that region is not near vacuum at this time. After propagating past this filamentation point, the pulse underwent self-focusing and propagated forward into the plasma. By the time the pulse reached the left edge of the simulation box, there is virtually no displacement of the centroid, showing that beyond the initial filamentation, there was virtually no hosing apparent in this simulation.

An improvement over the radial density profile simulations matches our expectations. Should a pulse be displaced slightly from its original vertical positioning in this planar exponential profile, it would still see an approximately symmetrical density profile about its centroid. However, the radial density gradient in previous

sections introduce a transverse density asymmetry to a pulse displaced from its original position. Should a pulse in the radial profile be displaced, the side closest to its original path would see a higher average density than the far side, resulting in a phase velocity gradient where the outer edge has a lower phase velocity than the inner edge, thereby leading to significant hosing away from the window center. This implies that in lower driver energy experiments, one could expect to see more hosing since the density profile will have much greater curvature than higher energy experiments.

7. Summary

In this paper, an expanded physical model for relativistic laser hole-boring in plasmas has been presented and verified against two-dimensional large-scale particle-in-cell simulations. The results show for the first time analytically that the effects of the hosing instability do indeed increase as a function of density. However, this is mitigated by the use of strongly relativistic laser pulses where enormous ponderomotive pressure is able to quickly self-correct the channel deviations.

This is illustrated throughout the hole-boring simulations of section 6 which utilizes highly relativistic, $a_0 = 20$, intensities. These simulations were initially designed to determine if the multiple pulse improvements found in [41, 42] can be realized on modern day facilities such as Vulcan Petawatt, OMEGA EP, and NIF ARC. The results show that while the multiple pulse method is indeed effective with short enough pulses, the duration and shape of the pulses required is not feasible with neodymium-based laser technology. In fact, using multiple pulses in this parameter regime can even worsen the levels of hosing due to the dependence on density as derived in section 3 and verified in section 5.

Additionally, it has been shown that the ponderomotive force is great enough at these high intensities for the pulses to quickly self-correct, resulting in no appreciable displacement by the end of the simulation. This self-correction occurs faster at higher intensities, thereby reducing the energy losses to the hosed filaments.

Further, the effects of the density profile on the hosing instability have been explored, showing that more radial profiles lead to additional hosing. This implies that larger-scale experiments which have more planar density profiles about the critical density should experience less holding than their lower energy counterparts.

All of this is in line with the physical model presented in the theory portion of this paper, thereby showing that increasing the laser intensity of the channeling pulse is a viable approach to hole-boring. Not only are higher intensities predicted to allow straighter, more controlled channels through realistic density profiles by overcoming the density asymmetries inherent in plasmas, but recent research has shown that they are also expected to seed magnetic fields to help collimate subsequent fast electron beams generated by trailing pulses [62], thereby illustrating the promise and need for development of this branch of relativistic high energy density physics research.

Additional work is currently underway to further explore the parameter space surrounding the hosing instability with focuses on the frequency dependence of the hosing equation as well as the effects of exotic polarizations. The results of these investigations are to be submitted upon completion of a full analysis.

Acknowledgments

The authors would like to thank the OSIRIS consortium for the use of OSIRIS. We would also like to thank the staff of the Central Laser Facility and the Computer Science Department at the Rutherford Appleton Laboratory for the use of the SCARF-LEXICON computer cluster, as well as the ARCHER UK National Supercomputing Service. MCL thanks the Royal Society Newton International Fellowship for support. This work has been carried out within the framework of the EUROfusion Consortium and has received funding from the Euratom research and training programme 2014–2018 under grant agreement No 633053. The views and opinions expressed herein do not necessarily reflect those of the European Commission. The authors further acknowledge the support of the Plasma HEC Consortium, EPSRC Grant #EP/L00023711 as well as additional grant support from STFC Grant #ST/M007375/1.

Appendix. Simulation Validation

The simulations in section 6 utilized cell sizes of approximately three times the Debye length and density profiles that increased towards the absorbing walls of the simulation window. As a result, it is necessary to check for any unphysical effects that could be caused by artificial heating or edge effects. To accomplish this, additional simulations were run using identical profiles to the radial density profiles in section 6.

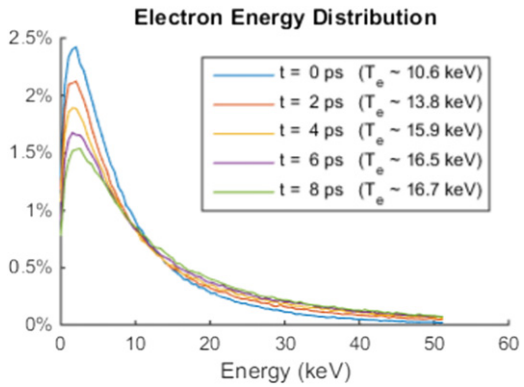

Figure 11. The energy spectrum of the plasmas used in section 6 with no lasers incident. Significant artificial heating can be seen over the length of the simulation.

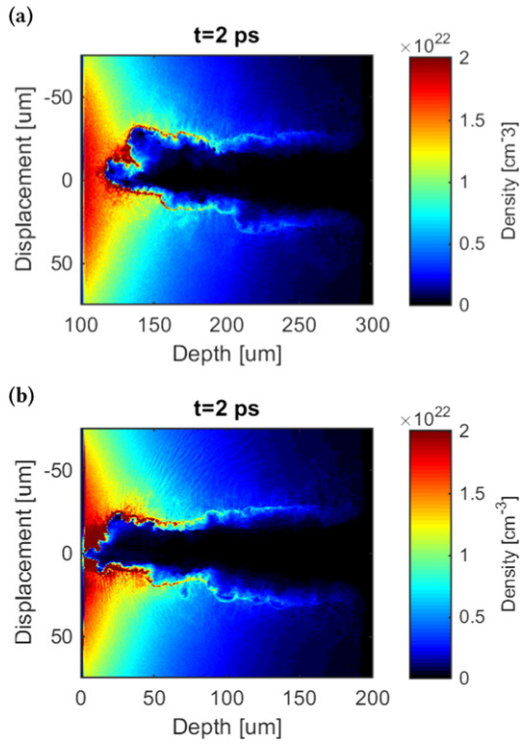

Figure 12. Convergence test of the single pulse simulation in section 6. The electron density profile is shown after 2 ps of simulation time in (a) the original simulation presented in section 6 and (b) the identical simulation run with double resolution.

To check for artificial heating, a simulation was run matching the radial density profile simulations in section 6 but with no laser pulses incident on the plasma. The energy of the particles was binned and the tail of the energy spectrum was fit by the Boltzmann distribution in order to determine the heating of the plasma. The results are shown in figure 11. As can be seen, significant heating of the plasma was observed in the absense of a laser pulse, and so a convergence test was run.

The spatial grid of the single pulse simulation in section 6 was set to 20 000 × 15 000 cells in order to halve the cell size and check for any effects from the observed artificial heating. The results of this simulation are shown in figure 12. While the results of these two simulations do not exactly match, similar features are seen in both, particularly the initial hosing of the pulse away from the high-density region and the ponderomotive self-correction. Due to the stochastic nature of the hosing instability, a change in the absolute shape of the channel is to be expected. Therefore it was determined that the simulations used in previous section were sufficient to illustrate the effects of pulse number and geometry on the hosing instability.

Additionally, as part of the original investigation, simulations were also run at intensities corresponding $a_0 = 3$ with the simulation window starting from $z = 192.2$ μm in order to reach the same relativistic critical

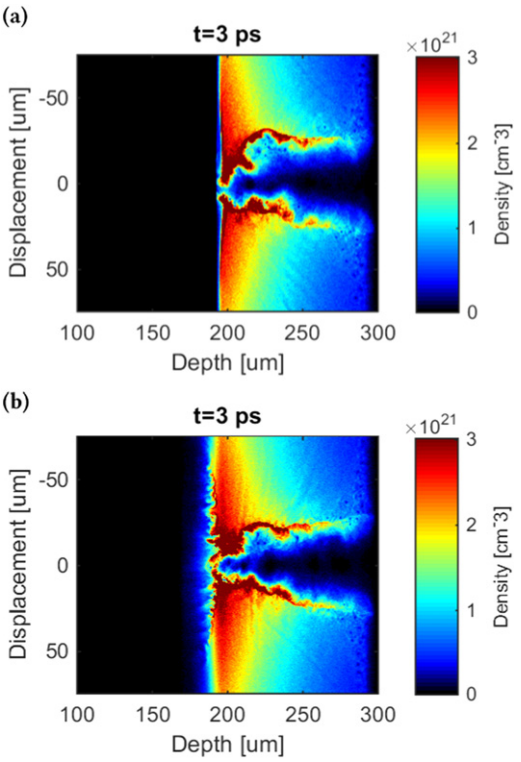

Figure 13. Edge effects test of the $a_0 = 3$ single pulse simulations. The electron density profiles are shown (a) with an absorbing edge at $z = 192.2$ and (b) with an exponential downramp starting at $z = 192.2$.

maximum as the $a_0 = 20$ cases. The ponderomotive self-correction was still present at this intensity, though a greater percentage of the pulse's energy was diverted into the hosing channel. Since this simulation still exhibited the same features discussed in section 6, the artificial heating will have no strong impact on the analysis presented above.

In order to test for these artificial effects, an additional $a_0 = 3$ simulation was run with an added 10 μm, 2 μm scale length exponential decrease in density added behind the previous absorbing edge. The resulting electron density profiles of these simulations is shown in figure 13. Here again, while the absolute shapes of the channels differ, this is to be expected, and the major features of hosing away from high-density regions and ponderomotive self-correction are still present.

Therefore, since both artificial heating and edge effects do not greatly alter the simulations presented above, the results of these simulations are valid.

References

[1] Sprangle P, Esarey E, Krall J and Joyce G 1992 *Phys. Rev. Lett.* **69** 2200
[2] Tajima T and Dawson J M 1979 *Phys. Rev. Lett.* **43** 267
[3] Esarey E, Sprangle P, Krall J, Ting A and Joyce G 1993 *Phys. Fluids* B **5** 2690
[4] Wilks S C 1993 *Phys. Fluids* B **5** 2603
[5] Naumova N *et al* 2009 *Phys. Rev. Lett.* **102** 1
[6] Robinson A P L 2011 *Phys. Plasmas* **18** 18
[7] Robinson A P L, Trines R M G M, Dover N P and Najmudin Z 2012 *Plasma Phys. Control. Fusion* **54** 115001
[8] Pogorelsky I V *et al* 2012 *AIP Conf. Proc.* **1507** 814
[9] Wu D *et al* 2013 *Phys. Plasmas* **20** 023102
[10] Nerush E N and Kostyukov I Y 2015 *Plasma Phys. Control. Fusion* **57** 035007
[11] Kneip S *et al* 2008 *Phys. Rev. Lett.* **100** 1
[12] Faure J *et al* 2006 *Nature* **444** 737
[13] Leemans W P *et al* 2006 *Nat. Phys.* **2** 696
[14] Nakamura K *et al* 2007 *Phys. Plasmas* **14** 056708
[15] Matsuoka T *et al* 2009 *Plasma Phys. Control. Fusion* **51** 095003
[16] Tabak M *et al* 1994 *Phys. Plasmas* **1** 1626
[17] Hurricane O A *et al* 2014 *Nature* **506** 343
[18] Ma T *et al* 2013 *Phys. Rev. Lett.* **111** 085004
[19] Park H-S *et al* 2014 *Phys. Rev. Lett.* **112** 055001

[20] Atzeni S and Vehn J Meyer-ter 2004 *The Physics of Inertial Fusion: Beam Plasma Interaction, Hydrodynamics, Hot Dense Matter* (Oxford: Oxford University Press)
[21] Mulser P and Schneider R 2004 *Laser Part. Beams* **22** 157–62
[22] Tabak M, Norreys P A, Tikhonchuk V T and Tanaka K A 2014 *Nucl. Fusion* **54** 054001
[23] Cai H B *et al* 2014 *High Power Laser Science and Engineering* **2** e6
[24] Kodama R *et al* 2001 *Nature* **412** 798
[25] Kemp A J *et al* 2014 *Nucl. Fusion* **54** 054002
[26] Robinson A P L *et al* 2014 *Nucl. Fusion* **54** 054003
[27] Bellei C *et al* 2013 *Phys. Plasmas* **20** 052704
[28] Debayle A, Honrubia J J, D'Humières E and Tikhonchuk V T 2010 *Phys. Rev.* E **82** 036405
[29] Norreys P A *et al* 2014 *Nucl. Fusion* **54** 054004
[30] Krushelnick K *et al* 1997 *Phys. Rev. Lett.* **78** 4047
[31] Durfee C and Milchberg H M 1993 *Phys. Rev. Lett.* **71** 2409
[32] Willingale L *et al* 2011 *Phys. Rev. Lett.* **106** 105002
[33] Willingale L *et al* 2013 *New J. Phys.* **15** 025023
[34] Pukhov A and Vehn J Meyer-ter 1997 *Phys. Rev. Lett.* **79** 2686
[35] Weng S M, Murakami M, Mulser P and Sheng Z M 2012 *New J. Phys.* **14** 063026
[36] Kodama R *et al* 1996 *Phys. Rev. Lett.* **77** 4906
[37] Li G *et al* 2008 *Phys. Rev. Lett.* **100** 125002
[38] Sarri G *et al* 2010 *Phys. Plasmas* **17** 113303
[39] Najmudin Z *et al* 2003 *Phys. Plasmas* **10** 438
[40] Chen L M *et al* 2007 *Phys. Plasmas* **14** 040703
[41] Lei A *et al* 2009 *Phys. Plasmas* **16** 056307
[42] Yu W *et al* 2009 *Laser Part. Beams* **27** 109
[43] ARCHER UK National Supercomputing Services (http://archer.ac.uk)
[44] Cattani F, Kim A, Anderson D and Lisak M 2001 *Phys. Rev.* E **64** 016412
[45] Kim A, Tushentsov M, Cattani F, Andersen D and Lisak M 2002 *Phys. Rev.* E **65** 036416
[46] Naseri N, Pesme D, Rozmus W and Popov K 2012 *Phys. Rev. Lett.* **108** 1
[47] Kruer W L, Valeo E J and Estabrook K G 1975 *Phys. Rev. Lett.* **35** 1076
[48] Wilks S C, Kruer W L, Tabak M and Langdon A B 1992 *Phys. Rev. Lett.* **69** 1383
[49] Kruer W L and Wilks S C 2000 *Plasma Phys. Control. Fusion* **34** 2061
[50] Robinson A P L *et al* 2009 *Plasma Phys. Control. Fusion* **51** 024004
[51] Ping Y *et al* 2012 *Phys. Rev. Lett.* **109** 1
[52] Levy M C, Wilks S C, Tabak M and Baring M G 2013 *Phys. Plasmas* **20** 103101
[53] Levy M C, Wilks S C, Tabak M, Libby S B and Baring M G 2014 *Nat. Commun.* **5** 4149
[54] Willingale L *et al* 2009 *Phys. Rev. Lett.* **102** 125002
[55] Sarri G *et al* 2010 *Phys. Rev. Lett.* **105** 175007
[56] Bulanov S, Esirkepov T, Naumova N, Pegoraro F and Vshivkov V 1999 *Phys. Rev. Lett.* **82** 3440
[57] Farina D and Bulanov S V 2001 *Plasma Phys. Rep.* **27** 641–51
[58] Sarri G *et al* 2011 *Phys. Plasmas* **18** 23
[59] Esirkepov T, Nishihara K, Bulanov S V and Pegoraro F 2002 *Phys. Rev. Lett.* **89** 275002
[60] Singh D K, Davies J R, Sarri G, Fiúza F and Silva L O 2012 *Phys. Plasmas* **19** 073111
[61] Ren C and Mori W B 2001 *Phys. Plasmas* **8** 3118
[62] Scott R H H *et al* 2012 *Phys. Plasmas* **19** 053104
[63] Dias J M *et al* 1996 *Phys. Rev. Lett.* **78** 4773
[64] Epperlein E 1990 *Phys. Rev. Lett.* **65** 2145
[65] Mori W B 1997 *IEEE J. Quantum Electron.* **33** 1942
[66] Forslund D W, Kindel J M and Lindman E L 1975 *Phys. Fluids* **18** 1017
[67] Duda B and Mori W B 2000 *Phys. Rev.* E **61** 1925
[68] Kaluza M C *et al* 2010 *Phys. Rev. Lett.* **105** 095003
[69] Duda B J, Hemker R G, Tzeng K C and Mori W B 1999 *Phys. Rev. Lett.* **83** 1978
[70] Li G, Yan R, Ren C, Tonge J and Mori W B 2011 *Phys. Plasmas* **18** 042703
[71] Bulanov S V and Pegoraro F 2002 *Phys. Rev.* E **65** 066405
[72] Bulanov S V, Inovenkov I N, Kirsanov V I, Naumova N M and Sakharov A S 1992 *Phys. Fluids* B **4** 1935
[73] Matsuoka T *et al* 2008 *Plasma Phys. Control. Fusion* **50** 105011